# Neural Synchrony Links Sensorimotor Cortices in a Network for Facial Motor Control

Yuriria Vázquez[1,2 *], Geena R. Ianni[1,3*], Elie Rassi[4,5], Adam G. Rouse[6], Marc H. Schieber[7], Faraz Yazdani[1], Yifat Prut[8], Winrich A. Freiwald[1]

1. Laboratory of Neural Systems, The Rockefeller University, NYC, USA.

2. Laboratory of Sensory Neuroscience, The Rockefeller University, NYC, USA.

3. Hospital of the University of Pennsylvania, Department of Medicine, Philadelphia, PA, USA.

4. Donders Institute for Brain, Cognition, and Behaviour, Radboud University, Nijmegen, The Netherlands.

5. Department of Psychology and Centre for Cognitive Neuroscience, University of Salzburg, Salzburg, Austria.

6. Department of Neurosurgery, Department of Cell Biology & Physiology, University of Kansas Medical Center, Kansas City, KS, USA

7. University of Rochester Medical Center, Rochester, New York, USA

8. Edmond & Lily Safra Center for Brain Sciences, Jerusalem, Israel.

* These authors contributed equally to this work.

**Keywords:** facial expressions | oscillations | motor control | network | primates

**Correspondence:**

Yuriria Vázquez: yvazquez@rockfeller.edu;

Winrich Freiwald: wfreiwald@rockefeller.edu;

Yifat Prut: yifat.prut@mail.huji.ac.il.

## In Brief

Primates communicate through facial expressions. How the brain generates facial expressions remains poorly understood. To assess this question, we used fMRI-targeted electrophysiology and intracortical stimulation (ICMS) while non-human primates elicited different facial movements.

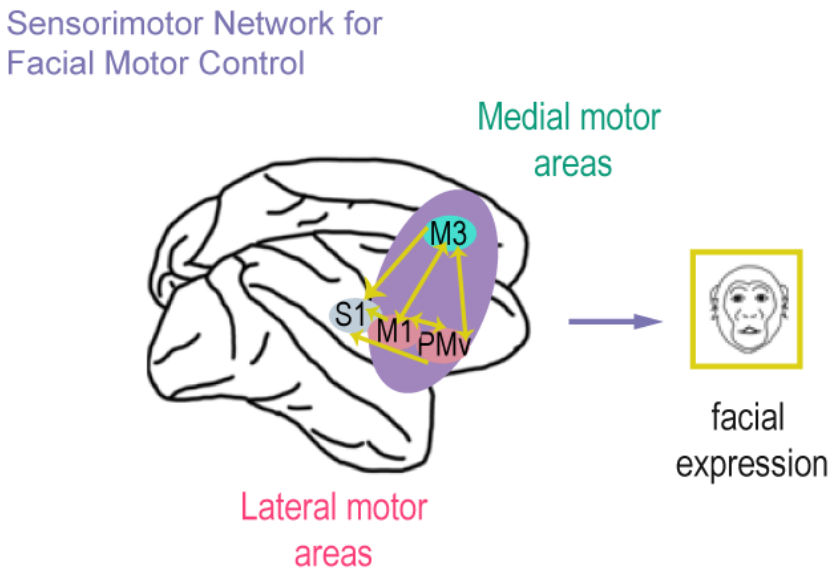


## Highlights

- ICMS revealed that medial and lateral face motor-related cortical areas can exert significant functional impact on each other.
- We identified functional interactions through specific frequency coupling among medial and lateral face motor areas, and S1 during the production of facial expressions.
- Medial and lateral face motor-related cortical areas form an interconnected network with the primary somatosensory cortex.
- Our results suggest that facial expressions could emerge from a sensorimotor network with dynamic and flexible connectivity that adapts based on the facial movement.

## Abstract

Primate societies rely on the production and interpretation of social signals, in particular those displayed by the face. Facial movements are controlled, according to the dominant neuropsychological schema, by two separate circuits, one originating in medial frontal cortex controlling emotional expressions, and a second one originating in lateral motor and premotor areas controlling voluntary facial movements. Despite this functional dichotomy, cortical anatomy suggests that medial and lateral areas are directly connected and may thus operate as a single network. Here we test these contrasting hypotheses through structural and functional magnetic resonance imaging (fMRI) guided electrical stimulation and simultaneous multi-channel recordings from key face motor areas in the macaque monkey brain. These areas include medial face motor area M3 (located in the anterior cingulate cortex); two lateral face-related motor areas: M1 (primary motor) and PMv (ventrolateral premotor); and S1 (primary somatosensory cortex). Cortical responses evoked by intracortical stimulation revealed that medial and lateral areas can exert significant functional impact on each other. Simultaneous recordings of local field potentials in all face motor areas further confirm that during facial expressions, medial and lateral face motor areas significantly interact, primarily in the alpha and beta frequency ranges. These functional interactions varied across different types of facial movements. Thus, contrary to the dominant neuropsychological dogma, control of facial movements is not mediated through independent (medial/lateral) functional streams, but results from an extensive interacting sensorimotor network.

## Introduction

In primate societies, individuals thrive with their ability to interpret and produce social signals. Primates communicate socially through vocalizations, speech, and facial expressions, all of which require precise control of facial musculature[1]. Facial expressions convey information about internal states or intentions, and thereby function as social signals among conspecifics. Despite the significance of facial expressions in social interactions, little is understood about the neural mechanisms underlying these social motor behaviors when compared to other motor actions such as reaching or grasping [2,3,4].

The primate brain harbors several cortical regions dedicated to facial motor control within the frontal cortex –specifically, the primary motor (M1) and the ventrolateral premotor (PMv) cortices on the lateral aspect, as well as the supplementary (M2) and the cingulate (rostral M3 and caudal M4) motor cortices on the medial aspect [5, 6]. Significantly, each of these cortical areas project directly to the facial motor nucleus in the brain stem [7], suggesting that motor cortical areas exert direct control over facial motoneurons in a seemingly parallel, independent control strategy, where each cortical area directly controls a subset of facial muscles.

Studies in human patients have shed light on the functional circuitry of these areas during facial expressions. Two facial areas (M1 and PMv) reside laterally, in the territory of the middle cerebral artery, and three areas (M2, M3, M4) reside medially, in the territory of the anterior cerebral artery [5]. Patients with middle cerebral artery strokes experience asymmetry in voluntary or goal-directed facial movements (performed in response to verbal commands), yet their ability to perform spontaneous emotional gestures like smiling remains intact[10]. In contrast, patients with anterior cerebral artery strokes (affecting medial motor areas) can execute normal voluntary facial movements, but struggle with emotional facial gestures[10]. These findings led to the neuropsychological schema that facial movements are controlled by two distinct pathways: lateral and medial motor pathways (Fig.1A) [8,9,10], each controlling a qualitatively different type of facial movement. This is further supported by the unique input and output connectivity patterns of the medial and lateral motor areas of the face. On the other hand, anatomical studies have identified corticocortical connectivity between medial and lateral motor areas of the face [7,11,12,13,14], including the facial representation in the somatosensory cortex[5]. Consistent with this, brain-wide imaging studies in non-human primates reveal that orofacial movements recruit a distributed network of cortical regions, implicating both medial and lateral motor regions for both types of facial gestures [15].

One possible way to reconcile the discrepancies between the human lesion studies, which suggest distinct roles for different cortical areas, and the data from anatomical and imagining

studies is by considering that the face motor areas form an interconnected network characterized by synchronized neural activity exhibiting dynamic expression-selective activity states that are coordinated across the network nodes (Fig. 1B). These network interactions may occur faster than fMRI's temporal resolution, limiting their capture with this technique. To test this hypothesis, we implanted recording arrays in fMRI-identified cortical areas of the facial motor and somatosensory areas of non-human primates. To capture interareal connectivity, we delivered intracortical microstimulation (ICMS) to one brain area while simultaneously recording the evoked local field potentials (LFPs) in the other areas. We further measured synchronous patterns in the local field potential (LFPs) among the multiple face motor areas and the primary somatosensory cortex (S1) to assess functional connectivity.

Our findings reveal that face motor areas indeed function as an interconnected network where medial and lateral areas exert significant influence on each other, as shown through our ICMS approach. During emotional facial expressions, we observed alpha and beta synchronization between medial motor area M3, lateral areas (M1 and PMv) and the face representation in primary somatosensory cortex, suggesting the presence of dynamic, expression-selective activity states coordinated across network nodes. This sensorimotor network's inter-areal dynamics displayed different patterns of functional connectivity that correlated with specific facial gestures, supporting our hypothesis that face motor areas and S1 form an interconnected network with flexible interactions based on synchronized neural activity that generates diverse neural patterns for different facial expressions.

## Results

We recorded LFPs from multiple channels (n=32 channels per area) located in the sensorimotor areas of the face, including the - primary somatosensory cortex (S1), primary motor cortex (M1), ventrolateral premotor cortex (PMv) and cingulate motor cortex (M3) – as head-fixed monkeys produced ethologically relevant facial movements in response to various stimuli (see Methods, Fig. 1C-D and Fig. S1).

### Estimating evoked inter-areal connectivity in the facial motor system

To identify connectivity patterns between facial motor areas, we employed intracortical microstimulation (ICMS) while the animal was sitting quietly, making no facial movements. For this purpose, we injected single pulse biphasic stimuli (250 μA, biphasic pulse duration of 0.4 ms, 300 Hz) through dedicated stimulation electrodes embedded in the recording arrays and measured the

evoked LFP (eLFP) recorded in neighboring arrays (Fig. 2A). Net signal propagation was assessed by analyzing the eLFP amplitude and waveform in receiving areas. Key measurements included the response magnitude, calculated as the difference between either the first peak and trough or the first trough and peak following the stimulation pulse (see Methods section for details).

Figure 2B shows the average area-specific eLFP obtained in response to microstimulation applied in M3, M1, PMv and S1 areas, obtained across several recording sessions (n ≥ 4200 stimulation pulses). We found clear evidence for signal propagating from the medial (M3) to the lateral (M1 and PMv) motor areas, and the primary somatosensory cortex (S1). The eLFP responses obtained in S1 (purple line) were generally smaller in amplitude and delayed by ~10 ms relative to the ones in the lateral motor areas (red and orange lines) suggesting slower propagation to this region (Fig. 2B, upper left panel). Nonetheless, we found that ICMS in all tested areas produced significant eLFP responses in all receiving areas, though with varying magnitudes and waveforms. We quantified the evoked connectivity between brain regions using a connectivity matrix (Fig. 2C). This matrix revealed several key patterns, notably a strong reciprocal connection between M1 and S1 [16]. M3 received inputs from both lateral motor areas (M1 and PMv), with M1 eliciting a larger response than PMv. The response to primary somatosensory (S1) stimulation was comparatively smaller. When stimulation was applied to M3, both lateral motor areas responded (M1 and PMV), aligning with previously described anatomically connectivity patterns[5]. However, an asymmetry was observed: while M3 stimulation produced relatively modest responses in all areas, stimulation of M1 evoked strong responses in M3. This asymmetry could potentially be explained by orthodromic activation of the source area during local stimulation.

This set of results validates the use of eLFP for identifying anatomically relevant functional connectivity across different cortical areas and suggests that the observed medial-to-lateral connectivity reveals physiologically relevant pathways between these network components.

**LFP Synchrony Links Sensorimotor Cortices in a Network for Facial Motor Control**

Since evoked responses to stimulation may provide a biased estimate of the ongoing interareal interactions we assessed functional connectivity by calculating the synchronization of LFP signals when monkeys perform different facial gestures, allowing us to examine how these interareal interactions are modulated by specific behavioral contexts. Previous studies have already shown that LFP signals can provide insights into the neural processes underpinning various cognitive functions and actions [17, 18, 19]. We used long stretches of LFP recordings (7-10 minutes) and identified movement pattern and timing using manual scoring and an automatic algorithm based on the calculated optic flow (see Methods). Functional connectivity was assessed using

pairwise phase coherency (PPC) between the LFPs of the recorded areas, quantifying the distribution of phase differences [20]. This method assumes that neural synchronization between two areas will show a distribution of phase differences centered around a mean value. Our connectivity analysis specifically targeted the movement execution period, which enhances our ability to accurately define distinct actions. The analysis first examines differences in functional connectivity patterns between periods of facial stillness (rest) and movement. We found clear differences in the functional connectivity when the face was still compared to when it moved. Overall, during emotional behaviors, beta-range (13-40 Hz) connectivity between lateral and medial motor areas (M1 and M3) increased during movement. The M3-PMv connectivity, however, showed behavior-specific patterns: it increased in the beta range during lipsmacks but decreased during threats. For voluntary movements (chews), the medial-to-lateral connectivity shifted toward lower frequencies, showing increased theta (5-7 Hz) and alpha (8-12 Hz) connectivity while beta connectivity diminished during movement execution. Regarding lateral motor areas connectivity, both emotional and voluntary movements showed increased M1-PMv beta band connectivity during movement compared to rest, with voluntary movements additionally exhibiting enhanced theta and alpha connectivity (for details see Table S1, cluster-based nonparametric statistics with dependent samples t-test, $p <= 0.05$).

While the above analysis revealed general patterns of functional connectivity that point to movement-related modulation between these areas, our main analysis focused on understanding the movement-specific functional interactions between the sensorimotor face areas, as well as characterizing the directional flow of information within the network during different types of facial movements. We first calculated functional interactions between medial and lateral motor areas during threats (red) and lipsmacks (LS - yellow), representing emotionally based gestures with opposite valence (Fig. 3A-C). In general, synchrony appears to be frequency-dependent, but consistently stronger during threats compared to lipsmacks. Statistical analyses revealed that the threat-related interareal synchrony was significantly stronger than the synchrony level during lipsmacks, mostly in the low frequency range (thick shades in Fig. 3A-C; cluster-based nonparametric statistics with dependent samples t-test, $p <= 0.05$, see Table S2) but not in the high-frequency range (i.e., beta range). Interestingly, the functional interactions between the medial (M3) and lateral (M1 or PMv) motor systems during emotional facial movements (depicted in Fig. 3A-B) were comparable in properties but weaker in magnitude compared to the interactions within the lateral subnetwork (M1 and PMV in Fig. 3C). In both cases, the synchrony during threats was stronger than during lipsmacks mostly in the low-frequency range (<20 Hz).

Beyond motor system interactions, we investigated how primary somatosensory cortex (S1) functionally connects with motor areas during different emotional gestures, providing insight

into sensorimotor integration. We observed beta synchrony between S1 and both medial (M3) and lateral motor areas, with a clear broad peak in the beta frequency range for functional connectivity between S1 and PMv (Fig 3D-E) during threats and lipsmacks. Similar to patterns within the motor network, coupling between S1 and motor areas, was consistently stronger during threats than during lipsmacks (Fig 3D-F). This gesture-specific synchrony pattern suggests functional differences beyond the distinct kinematics characterizing these two gestures.

Next, we compared the neural activity during emotional facial movements with that observed during voluntary, goal-directed facial movements (specifically, chewing movements). We found increased synchronization both between the lateral motor cortices (M1 and PMv), and between the medial and lateral motor cortices (M3 and M1, M3 and PMv) during chewing compared to rest (Table S1). Further analysis revealed consistent coupling within the lateral system (M1 and PMv) during both voluntary and emotional movements, with no significant differences detected (Fig. S2C, Table S2). However, during voluntary chewing, the M3 area showed synchronization with M1 and PMv mainly at low frequencies (4-8 Hz). In contrast, beta range synchronization was not prominent. In general, emotional movements elicited stronger alpha and beta coupling across the medial and lateral systems, illustrating distinct functional interactions during movement execution (Fig. S2A-C).

In summary, the lateral motor system (M1 and PMv) maintains consistent beta-frequency coupling during all movement types, with evident movement-specific differences mainly in the alpha range coupling between threats and lipsmacks. The medial-to-lateral connectivity (M3 to M1 & PMv) shows broader frequency-range variations that depend on the ongoing movement type: emotional movements engage primarily alpha and beta range, while voluntary chews show reduced synchronization in these bands and predominantly operate at lower frequencies (<10 Hz, Table1).

**Directional Information within the Face Sensorimotor Network**

Our findings have revealed a dynamic sensorimotor network where frequency coupling varies based on the type of facial movement. However, the synchrony measurement we used (PPC) cannot identify directionality of interactions. For this purpose, we employed Granger Causality analysis, which measures the extent to which activity in one area (e.g., variable X) can significantly predict subsequent activity in another area (e.g., variable Y) thereby hinting at causal relations (or “information flow”) between the two regions [21, 22]. We used Granger causality to reveal differences in the inter-areal information flow during different facial movements, with particular emphasis on information flow between medial and lateral areas of the facial motor system (M3 and M1 & PMv). Using this approach, we found bidirectional information flow between medial and lateral motor areas, with the magnitude of the flow varying according to the facial expression. When

comparing threats to lipsmacks, information flow from medial to lateral motor areas was stronger during threats, while flow in the opposite direction remained similar between both behaviors (Fig. 3G-H). Interestingly, the interactions with S1 were substantially more asymmetric, showing a consistently stronger flow of information from motor regions to S1 than in the reverse direction (Fig. 3J-L).

During voluntary movements, the coupling between the medial (M3) and lateral motor areas (M1 and PMv) was significantly weaker compared to emotional movements, while the coupling within the lateral cortices remained similar. Consequently, we observed significantly lower information flow from M3 to the lateral motor areas M1 and PMv during voluntary movements compared to threat-related emotional movements (Fig. S2D-E). Information flow in the opposite direction was minimal, with the exception of signals from the PMv area (Fig. S2E). Within the lateral system, higher information flow from M1 to PMv was detected during threats compared to voluntary chewing (Fig. S2F).

As shown in Figure 4, the network analysis reveals that motor areas show largely symmetric information flow (except for M3-to-M1 during threats, Fig. 4A), while motor-to-somatosensory information flow is predominantly unidirectional (Fig. 4A-B). While inter-areal synchrony was stronger within the lateral motor areas and weaker for medial-lateral motor interactions, information flow remains reliable across both medial and lateral regions, indicating continuous information exchange through the facial motor system (Fig. 4B). The pattern of differential synchrony strength coupled with reliable information exchange demonstrates how this sensorimotor network maintains flexible functional interactions. These interactions can be dynamically modulated to coordinate neural activity patterns underlying different facial gestures.

**Facial Movement-Specific Local Power Dynamics**

After identifying distinct connectivity and directionality patterns during emotional and voluntary facial movements, we investigated how local neural activity in each network area relates to facial gestures, focusing on oscillatory power modulations that reflect the local neural population activity. To investigate this, we analyzed the region-specific LFP dynamics.

Figure 5A and S3A-D, illustrates modulation in the raw local power across the different frequency bands (alpha: 8-12 Hz, beta:13-40 Hz and gamma 40-120 Hz) in lateral (M1 and PMv), medial (M3) and somatosensory (S1) areas during different emotional facial movements, analyzed from 1s pre- to 1s post-movement onset. Significant differences in the power between behaviors were confirmed by the Kruskal-Wallis test ($p<=0.01$, Table S4-S5), with each behavior showing distinct patterns of power modulation across regions.

To assess the temporal pattern of the LFP signals in different areas and varying facial movements we normalized the power of the ongoing oscillations during the movement period against the preparatory period (see Methods). In motor areas we found a ubiquitous pattern of beta-suppression as has been identified during voluntary movements of the upper limb [3,42]. Nonetheless the details of the suppression dynamics were movement and area-dependent (Fig. 5B).

In addition, we found in both M1 and M3 an increase in gamma power (≥ 40 Hz), during emotional and voluntary facial movements (Fig. S4E-G). In S1, beta suppression was modest, reaching significance only during chewing movements (Fig S3), while movement-related increases in alpha, high beta (>20 Hz), and gamma power, were dominant across all movement types.

In summary, our findings reveal area-specific oscillatory patterns reflecting distinct neural computations within each region. Activity in both medial and lateral face motor areas showed only subtle differentiation between emotional and voluntary movements. In contrast, we observed robust interareal synchronization based on consistent phase relationships predominantly in alpha/beta bands that varied systematically across different facial gestures. These synchronized interactions between medial area M3, lateral areas (M1, PMv), and S1 occurred with frequency-specific coupling patterns unique to each facial gesture. The magnitude and directionality of information flow within this network dynamically reconfigured depending on the type of facial movement.

## Discussion

In this study, we identified functional interactions between medial and lateral face motor areas and the primary somatosensory cortex during facial expressions in non-human primates—behaviors that are fundamental for social communication. Our results demonstrate a distributed cortical sensorimotor network that challenges the classical two-pathway model based on stroke patient studies [9, 10] and brain imaging research [23, 24], which proposes separate control circuits for emotional and voluntary facial movements. Instead, we found modulations in the local activity of both medial and lateral face motor areas for both types of movements. While there was only subtle differentiation in local activity between these movement types, we identify specific frequency coupling among these regions, suggesting that facial expressions could emerge from a sensorimotor network with dynamic and flexible connectivity that adapts based on the movement type.

Our findings reveal that medial and lateral motor cortices interact during facial expressions through specific inter-areal coupling. Despite their distinct local oscillatory signatures, these regions showed synchronized activation during emotional facial movements, demonstrating functional

interactions within an integrated motor network. Recent work[25] strengthens our interaction hypothesis by showing that in humans lateral motor areas receive emotional movement-related information, as evidenced by M1 activation during both voluntary speech production and emotional movements like smiling. Crucially, our ICMS connectivity results provide evidence for this network architecture, by revealing connectivity between medial and lateral motor face areas.

Neural communication among populations is mediated by their synchronous activity [26,18], which is fundamental for the dynamic coordination of distributed neural activity in local and extended networks underlying sensorimotor processes [27,28,29]. Information processing between distant neural assemblies depends on the strength of coherent activity through synchronous oscillations[30], with long range interactions involving a broader spectrum of frequency bands including theta, alpha and beta frequencies [31].

Our results, align with and extend these fundamental principles of neural communication, revealing specific patterns of synchrony between the neural populations of medial (M3) and lateral motor areas (M1 and PMv), as well as with the somatosensory cortex (S1) in the alpha and beta range, during facial expressions, extending into the theta range for voluntary chewing. The synchrony between areas, measured as phase relationships between the oscillations, was independent of changes in local power, and both the degree of synchrony and inter-area influence varied with the type of facial movement.

Alpha synchrony typically reflects the inhibition of task-irrelevant information [32,33], crucial for executive functions [30]. The patterns we observed in the face sensorimotor network align with this establish gating role. We found differential alpha coupling between lipsmacks and threats in key sensorimotor areas (medial-lateral: M3-PMV, M3-M1, M3-S1; lateral: M1-PMV, PMV-S1; Table S2) suggesting expression-specific synchrony modulations. This supports alpha's role in gating information based on context and attention[33]. The modulations in alpha synchrony across facial expressions likely regulates information flow during facial movements by suppressing irrelevant inputs while maintaining attention on motor behavior.

Complementing the role of alpha synchrony, beta synchrony plays a crucial role in the large-scale coupling of sensorimotor information[34]. Beta band coherency is ideally suited for flexibly and dynamically forming neural assemblies [35], and long-distance inter-area communication [31]. Beta oscillations can also be context-specific, reflecting current task rules or decisions [36,37]. In our case, shifts in the beta frequency peaks across different facial expressions (Fig 3A-B medial-lateral connectivity M3-M1, M3-PMv; Table 1) may contain information about the decision to perform specific facial movements in particular social contexts [37, 38] . The significance of beta synchrony extends beyond our specific findings. Previous research has demonstrated beta synchrony's

crucial role in synchronizing large-scale cortical networks in sensorimotor [39] and social decision-making tasks[40].

To understand how this synchrony-mediated coordination occurs, we examined information flow using Granger Causality analysis. Results showed continuous bidirectional exchange between medial and lateral motor regions, as well as among lateral regions, indicating dynamic information flow during facial expressions. We observed behavior-specific asymmetries, such as enhanced information flow from medial area M3 to lateral motor area M1 during threats. This asymmetry might reflect the unique demands of threat displays, which require sustained, non-affiliative movements that may depend more heavily on M3 control, unlike the affiliative and rhythmic patterns of lipsmacks in which the M3-to-M1 information flow was attenuated. Importantly, while we categorized lipsmacks as emotional movements, research suggest that they may be evolutionary precursors of human speech, potentially incorporating both emotional and voluntary control components [50.] This dual nature, along with the opposing valence of between threats and lipsmacks, may contribute to the observed asymmetric information flow pattern from medial to lateral areas. In contrast, PMv, showed symmetric information flow patterns between medial and lateral areas during both emotional movements, suggesting it could function as a central hub facilitating bidirectional information exchange (Fig. 3H-I) [51]. The primary somatosensory cortex exhibited asymmetric communication patterns, receiving more information from motor areas than it sent back. While this incoming flow might represent information about planned or ongoing movements [41], further studies are needed to test this hypothesis.

In summary, our findings reveal a dynamic cortical sensorimotor network with flexible connectivity that adapts based on the behavioral context and facial movement type. Intracortical stimulation showed that medial and lateral areas exert significant functional impact on each other, while LFP recordings confirmed these regions interact primarily in alpha and beta frequency ranges during facial expressions. Rather than separate motor circuits for emotional and voluntary movements, our data suggest that facial control corresponds with coordinated inter-areal interactions within an extensive sensorimotor network, challenging the dominant neuropsychological dogma of independent medial/lateral streams. This network likely enhances signal coordination to the facial nucleus by integrating information across brain regions. Future work should examine how social context, and internal states modulate these interactions, and explore the integration of subcortical structures (thalamus, basal ganglia, amygdala and insular cortex) [15,43,44] with cortical networks.

## Materials and Methods

All animal housing, care, and all experimental procedures complied with the National Institutes of Health Guide for Care and Use of Laboratory Animals and were approved by the Institutional Animal Care and Use Committees of the Rockefeller University (protocol numbers 21104-H USDA) and Weill Cornell Medical College (protocol number 2010-0029).

### Subjects

We studied two male monkeys (Macaca fascicularis (M1) and Macaca mulatta (M2)) that were group -or pair housed in directly neighboring cages before and during the experiments.

A cranial implant composed of MR-compatible acrylic cements, anchored with MR-compatible ceramic screws was implanted in each subject following standard surgical methods, and standard anesthetic, aseptic and postoperative treatment protocols. A custom-designed MR-compatible headpost was fixed to each implant.

### fMRI Behavioral Task

Monkeys were trained to sit in a sphinx position and maintain passive fixation on a dot at the center of a screen for 2-4 seconds to receive fluid reward while blocks of pictures or videos were presented, interleaved with baseline periods during which only the fixation dot appeared. During imagining, the subjects sat in an MRI compatible NHP chair with the head fixed at isocenter. Gaze position was tracked at 120 Hz, with an MRI compatible eye-tracker. All behavioral and stimulus display parameters were controlled with Presentation Software (Neurobehavioral Systems). During the functional scans, video stimuli were projected at 60 Hz resolution on a back-projection screen placed 35 cm in front of the subject's eyes. Monkeys performed a social-interaction free-viewing task as described in Shepherd & Freiwald[15], and an oro-facial motor localizer in which sparse, intermittent fluid reward was delivered during a passive fixation task [45].

Facial movements were tracked at 15 Hz using an MRI-compatible infrared video camera (MRC), whose acquisition was synchronized with the first TR of each scan run. The onset and offset of the facial emotional (threats, lipsmacks), voluntary (chew, drinking) and other (yawn) movements was determined offline by two independent observers, manually annotated and cross-validated.

### fMRI Acquisition

Monkey2 was previously fMRI-mapped as described in Shepherd & Freiwald[15]. Monkey1 was scanned and fMRI mapped in a similar fashion. All MRI data were acquired in a 3T Siemens Prisma scanner, while monkeys were in sphinx position. Functional imaging was acquired using custom-designed surface 8 channel receiver radiofrequency coils and a horizontal single loop transmit coil (L. Wald, MGH, Martinos Center for Biomedical Imagining) in echoplanar imagining sequences (EPI: TR 2.25 s, TE=17 ms, Flip angle 79 degrees, 1.2 $mm^3$ isotropic voxels, FOV=96 mm). Matrix size= 80 X 80 X 45, horizontal interleaved slices, 2X GRAPA acceleration. Volumes per run ranged from 168 volumes per run.

Right before each scanning session, Molday ION (monocrystalline iron oxide nanoparticles) was injected into the saphenous vein below the knee to increase the contrast-to-noise ratio (CNR [46]). The dose ranged 9 mg/kg on an initial scan day to 6 mg/kg on subsequent scanning days.

Anatomical images were collected from each subject in a separate session while subjects were anesthetized (ketamine 5-8 mg/kg, isoflurane 0.5-2.0%, and dexmedetomidine 0.008-0.02mg/kg), and placed on an MR-compatible stereotactic frame. Images were acquired using a customized 1-channel receive coil (L. Wald, MGH, Martinos Center for Biomedical Imagining). Anatomical images were based on the averaged of 6 repetitions of a T1-weighted magnetization-prepared rapid gradient echo (MPRAGE) sequence (FOV 128 mm, voxel size 0.5 X 0.5 X 0.5 mm). A computed tomography (CT scan) of the head & neck was acquired on the same day, to provide high anatomical resolution of the skull and skin.

**fMRI Analysis and Face Sensorimotor Cortex Localization**

Imagining analysis was done with free Surfer and FS-FAST (v6.0), using customized MATLAB and Linux-shell scripts as described in Shepherd & Freiwald[15]. Raw image volumes were 2D (slice-wise) motion and time corrected (AFNI, 3dAllineate, version AFNI_2011_12_21_1014), aligned to high-resolution anatomical T1, unwarped (JIP Analysis Toolbox, v3.1), smoothed (2 mm Gaussian FWHM) and masked. The first four volumes of each functional run were excluded from further analysis.

We constructed two GLM models to localize the sensory and motor face cortical areas. The onset times of the manually scored facial expressions were convolved with the MION HRF to generate a primary regressor of interest that will result in a “face expression activity map”. In the second GLM model the times at which juice-was delivered, were used to create an “orofacial motor activity map”.

Average signal intensity maps for each contrast were computed with FS-FAST function selxavg3-sess. The MION HRF was modeled as a wide gamma function with a steep initial slope (delta = 0; tau = 8000; alpha = 0.3; dt = 1 ms) and discretized to the length of the TR (2.25 s), in order to be used as a regressor in the GLM. In both models, nuisance regressors included 2$^{nd}$ order polynomial for drift, and the top 3 head motion PCs obtained from 2D slice-wise motion correction (3DAllieniate). The resulting voxel-wise beta-weight maps were not further corrected for multiple comparisons.

Significant voxels in both maps were identified, with a conjunction analysis using logical ANDs, taking the least significant *p-value* from each contrast entered in the conjunction. The conjunction facial expression-orofacial motor map was used for surgical targeting. This reliably identified voxels primarily correlated with oro-facial movement, and not body movement which occasionally accompanied facial expressions during the social-interaction free viewing task.

Brain coordinates were transformed from RAS space to stereotaxic coordinates using the Saleem-Logothetis atlas[47] to verify target locations were within intended cortical areas for surgical implantation. Transformation aligned AC to +21mm from the interaural line, with coordinates calculated as distances from reference points: AP from AC (Y-axis), ML from midline (X-axis), and DV from ear bar zero (Z-axis).

Monkey 1 (M. fascicularis):

- Reference: AC [-0.18, 24.18, 19.28], PC [-0.18, 15.13, 18.94], EBZ [-0.52, 7.12, 12.01]

- DV adjusted with 1.14 scaling factor and +4.71mm offset for species differences
- Targets [RAS → AP/ML/DV mm]: S1: [21.49, 19.36, 26.46] → [+16.18/+21.67/+21.18] M1 medial: [20.79, 22.71, 26.98] → [+19.53/+20.97/+21.78] M1 lateral: [22.62, 22.69, 24.78] → [+19.51/+22.80/+19.27] PMv: [19.01, 30.32, 26.90] → [+27.14/+19.19/+21.68] M3: [3.99, 34.05, 30.98] → [+30.87/+4.17/+26.34]

Monkey 2 (M. mulatta):

- Reference: AC [-3.69, -3.01, 24.67], PC [-3.69, -16.91, 23.43], EBZ [-3.65, -24.38, 10.65]
- Targets [RAS → AP/ML/DV mm]: S1: [17.28, -8.88, 37.86] → [+15.13/+20.97/+27.21] M1: [17.25, -5.08, 37.86] → [+18.93/+20.94/+27.21] PMv: [18.43, 3.37, 33.38] → [+27.38/+22.12/+22.73] M3: [0.18, 7.78, 39.47] → [+31.79/+3.87/+28.82]

**fMRI-Guided Electrophysiological Recording sites**

We used CORTEXPLORER SCI, a commercially available integrated functional/structural MRI-based stereotaxic planning and intra-surgical tracking approach (cortEXplore GmbH, Linz Austria) to target the position of 6-8 FMAs (floating microarrays, Microprobes: https://microprobes.com/products/multichannel-arrays/array-comparison-chart) based on the fMRI facial expression-orofacial motor map, described above. We targeted the face representation in the following areas based on the fMRI map: primary somatosensory cortex (S1), primary motor cortex (M1), ventro-lateral premotor cortex (PMv) and rostral cingulate motor area (M3). All arrays were implanted in the right hemisphere of both animals (Fig. 1C and Fig. S1).

For each subject, we aligned all functional maps and a high-resolution CT to the anatomical MRI, creating a project with the images of the skin, skull, brain and functional maps. Thus, the surgical planning occurred in the subjects' native space. For each target, we defined a corresponding entry point on the cortical surface; together these two points define a 3D trajectory for the array implantation. Each FMA included electrodes of varying length to maximize gray matter neural activity recordings. Intraoperative, we registered the surgical subject with its radiological data in CORTEXPLORER SCI, under general anesthesia and sterile conditions. This process creates a spatial relationship between the 3D virtual image space and the 3D physical subject.

We registered the subject in two steps – first with seven fiducial markers on the subject's acrylic implant, and second, with a few hundred points collected from the real subject's surface, in which the probe scans the surface of the surgical subject, registering it to its corresponding virtual surface. For each subject, the registration error was <200 microns RMS. Based on the target coordinates in each animal, we performed craniotomies and durotomies to facilitate the implantation of the FMAs. Each FMA was loaded onto the optically tracked probe, aligned with a predefined trajectory, and advanced slowly into the cortex for implantation. In all cases the 3D angular error between the actual and predefined trajectories was <1 degree.

**Neural Recording Behavioral Task**

The experimental design consisted in random blocks (7-10 min/block) of head-fixed monkeys performing one of the following behaviors: rest, voluntary chew ingestive movements (C), and

emotional facial expressions i.e. threats (T) and lipsmacks (LS). During rest periods the animals were left to stay calm, hence moving the least possible. During chew blocks the animals were fed by one of the experimenters with pieces of fruits intermittently. Facial expressions were elicited using a battery of different stimuli: a) conspecific face stimuli related to the social interaction task[15], b) conspecific movie stimuli, c) monkey avatar, d) interactions with conspecifics and humans. To make sure animals will look at the videos, they were previously trained to perform active and passive fixation tasks. During experimental recordings, the reward tube was removed to prevent occlusion of the subject's mouth and disambiguate social expressions from ingestive movements.

All visual stimuli were presented, and behavior controlled using MonkeyLogic (v2.2), running on a Windows computer system which sent the triggers to the TDT (Tucker-Davis Technologies) data-acquisition system via an analog and digital input/output card PCIe-6343. Subjects viewed visual stimuli on a 56 x 24 cm (1024 x 768 resolution) screen at 58 cm from the eyes, with a refresh rate of 60 Hz. The conspecific movie stimuli were recorded with a GoPro7 camera attached to the monkeys' home cages. We extracted ten-second clips of monkeys engaging in social behaviors e.g. grooming and playing, and non-social behaviors e.g. eating, drinking, and idling. Videos contained one or two monkeys, either male or female, and a subset of these monkeys were familiar to the subject being recorded. Each clip was phase-scrambled (to control for low-level motion, color and luminance intensity). A single stimulus set shown during a single recording run consisted of 7-10 individual clips and their matched scrambles presented in a pseudo-random order.

For a subset of recordings, subjects viewed an interactive monkey avatar face. The avatar's facial movements were controlled by real-time tracking of the experimenter's face using an Optitrack system connected to a PC running Unity. The experimenter was in a separate room from the subject.

Every trial began with a variable period of required visual fixation, after which a video stimulus appeared; the subject was able to freely move his eyes to explore the videos as long as his gaze stayed within a virtual window the size of the frame of the video and additional 2 degrees surrounding it. No reward was given during these runs, and the reward tube was removed.

**Face and Eye Movements Recordings**

Facial movements and expressions were recorded using a FLIR BFS-US-13Y3 (http://softwareservices.flir.com/BFS-U3-13Y3/latest/Model/spec.html, monkey 1) camera at a video sampling rate of 70 Hz and a Flex 13 Optitrack system at 120Hz (https://optitrack.com/cameras/flex-13/, monkey 2) mounted ~70 cm away from the subject's face. All videos were black & white. Videos were captured by a dedicated Windows computer running Spinview (FLIR) or Motive (Optitrack). Video acquisition was synchronized with a TDT system using a TTL pulse. Eye movements were recorded using an ISCAN system and synchronized with the TDT (1.017 kHz) and Monkey Logic system.

**Electrophysiological Recordings**

Neural activity was recorded simultaneously using FMA arrays with 36 channels per array (FMA, Microprobes Inc) with spacing of 400 µm, and 4 x 1.8 mm dimensions. We recorded a total of 256 channels (M1) and 192 (M2) of 6-8 individual arrays implanted in the face representation of the following areas: S1, M1, PMv and the rostral motor cingulate (M3). In each array the electrode

length was customized for each area to maximize gray matter activity recordings. In monkey 1, we used for analysis the arrays localized in the medial regions for M1 and PMv since the signal to noise ratio, quality and modulation of the signal was better than for their lateral counterparts. Electrode lengths ranged from 1.2-2.8 mm in all sensory-motor areas (S1, M1, PMv), except for M3 (5-9 mm) which is a deeper structure. In addition, the lengths of the electrodes were staggered and increased towards the sulcus. Recording electrode impedances were ~ 0.5 MOhm (n=28), microstimulation electrode impedance ~ 10K and less than 10 K for ground (n=2) and reference (n=2) electrodes.

**Data Acquisition**

Neural activity was recorded at full bandwidth with a sampling frequency of 24 kHz, and a resolution of 16 bits using a Tucker-Davis Technologies (TDT) system RZ2 Biosignal Processor. Neural data and all behaviors were synchronously stored to disk together with the face videos and eye movements. Raw recordings were filtered offline to obtain LFP (1kHz).

**Functional Connectivity Paradigm**

In monkey 1, the paradigm consisted in applying a 0.05 s biphasic stimulation pulse (amplitude=200 μA, duration 0.4 ms, 50 repetitions per current) delivered at 300 Hz for two minutes through each of the stimulation electrodes. Current acquisition was done at 24 kHz. Neural activity was stored as described above. Each array contained four low impedance (~10K) electrodes evenly spaced across the array, and 28 recording electrodes.

We first pre-processed and cleaned the data by selecting per array the channels without noise, using this channel selection we averaged their LFPs, and then analyzed the averaged evoked LFP across repetitions (n=50 repetitions, 32 or less channels per array, n=3 days). Per recording day, normalization was achieved by calculating a z-score per recording electrode and array. The z-score was determined by the voltage of the given electrode minus the average voltage across all selected electrodes of the array divided by their standard deviation. All z-scores per array for all given days were averaged to get a grand-average day where the connectivity measurements were measured. Connectivity was measured by quantifying the amplitude of the evoked Local Field Potential (eLFP) response in the receiver area following current delivery from a sender area. We measured the absolute difference between successive peak and trough amplitudes ($\Delta$|Peak-Trough|) in the eLFP, beginning 3 ms after the intracranial stimulation (ICS) onset to avoid stimulation artifacts. These connectivity measurements were then represented in a confusion matrix.

**Behavioral Analysis**

Facial expressions, voluntary chewing movements and other facial movements, were manually scored by 3 human observers for one monkey. The onset of the facial movements was determined by the time at which the subject's mouth started to move preceded by one second of mouth stillness. For the other monkey, we used for half of the sessions a customized python based automatic detector for mouth movements, based on the optic flow of the recorded video. This automatic scoring method was based on the average magnitude of optical flow around the animal's mouth in the recorded video. For each session, a Gaussian mixture model estimating the average optical flow magnitude around the animal's mouth, was used to cluster the frames in two categories. One category involved small or no mouth movements at all, while the other category involved large movements. The period of a facial movement was defined as a large movement period (>30 ms), preceded and followed by non-movement or small movement period longer than 1 second. For validation, the automatic onsets were cross validated with manual scoring onsets.

**Spectral Analysis**

In both monkeys, the LFP data were bandpass filtered from 1-256 Hz and preprocessed to form a data structure containing all voltage recordings per channel within each array, the sampling rate, and all trials with their corresponding behavioral events. All voltages were analyzed in μV.

We used custom-built MATLAB R2023a code (the MathWorks Inc., Natick, Massachusetts, USA) and Fieldtrip toolbox (v20170101 [48]) to analyze the data. We analyzed a total of 13(T), 13(C) & 7 (LS) recording sessions. A band-stop filter in monkey 2 was applied to remove the line noise at 60 Hz and harmonics. Artefacts, dead channels, and trials containing artifacts related to movement or electronic interference were removed based on visual inspection of the data.

The voltage was re-referenced per array using the low impedance electrodes distributed across the array. Using a fast Fourier transform approach, we computed time frequency representations (TFR) of the power (5-120Hz). For the range of 5-40 Hz, we used an adaptive sliding time window 4 cycles long (Dt=4/f) multiplied with a Hanning taper. For higher frequencies (40-120Hz), we used multitapers sleepians in a 0.2 s window with +/- 10 Hz of smoothing. The windows moved in .05 s steps, from 1s before the movement onset to 1s after the movement execution. Per type of facial movement condition i.e., threat, lipsmack or chew we averaged over trials within each recording session and then normalized by an absolute baseline subtraction using a 0.75 s window before movement onset. For visualization purposes, a grand average was computed over the recording sites (per area). In the case of the raw power, a similar analysis was performed, except for the normalization. Statistical analysis – see below, were computed using the raw power.

**Connectivity analysis**

We measured functional connectivity between the pairs of recorded areas by computing the pairwise phase consistency (PPC) measurement as implemented in Fieldtrip [20,48]. The PPC is an unbiased and consistent estimate of how well two signals generated by two sources show a consistent phase relationship in a particular frequency band (5-50 Hz). The advantage of using PPC versus other connectivity measurements is: 1) it remains reliable even with few trials, and 2) it is less prone to errors that occur when the consistency of phase differences correlates with the strength of the signal [20]. We focused the connectivity analysis on the movement execution period, to maximize the number of trials and certainty about the nature of the ongoing facial movement. By this we mean, for a given behavior e.g. lipsmacks, we split the full movement period into several epochs of 0.5 s duration. Each 0.5 s epoch during movement was used as trial for that given behavior. Movement lasting less than 0.5 s were discarded. We equalized the number of trials for calculating and comparing functional connectivity and Granger (see below) across behaviors, to avoid sample biases e.g. threats *vs* lipsmacks (n=1200), chews *vs* threats (n=4979).

As a first approach, we calculated the connectivity (PPC) of the network when the face was at rest, i.e. not moving or planning to move and compared it with the connectivity when the face was moving. Statistical differences within this contrast were assessed by a cluster-based nonparametric randomization[47], with a dependent samples t-test as statistic (see methods Statistical Analysis)

We used bivariate, nonparametric Granger Causality as implemented in Fieldtrip during the movement period to investigate the directionality of the connectivity[49] during the movement epoch.

**Statistical Analysis**

Differences in the average raw power across behaviors were calculated using a Kruskal-Wallis test, corrected for multiple comparisons ($p<=0.01$). The asterisks in Fig. 4A-D and Fig. S4A-D denote significant differences in the mean power between threats and other behaviors. However, all the performed comparisons are depicted in Table S4.

In the case of the Time Frequency Representation (TFR), statistical differences in the power were assessed comparing a window of 0.5 s before the movement onset (-0.75s to -0.25s) versus 0.5 s time window during the movement execution (0s to 0.5s).

We applied a cluster-based nonparametric randomization[48], with a dependent samples t-test to establish whether there were significant differences between two conditions (e.g. pre-movement vs movement epoch, or lipsmacks vs threats) in terms of power, PPC or Granger causality. By clustering neighboring samples (time-frequency points that show the same effect), this statistical test deals with the multiple-comparisons problem while accounting for the dependency of the data. All samples for which this t-value exceeded a prior threshold (uncorrected $p<=0.05$) were selected and subsequently clustered based on temporal-spectral adjacency. The sum of the t-values within a cluster was used as the cluster-level statistic. This was computed within all recording sessions (separately per area). By randomizing the data across the two conditions and recalculating the test statistic 1000 times, we obtained a null distribution of maximum cluster t-values to evaluate the statistic of the data ($p<=0.05$).

**Code Availability**

Code use for analysis will be deposited upon publication.

**Data Availability**

Data will be deposited upon publication.

**Editorial Assistance**

We used the AI-based language model, ChatGPT v4 by OpenAI and Claude 3.5 Sonnet, for English language editing to enhance manuscript clarity and readability. This comprises suggestions for sentence restructuring and phrasing improvements. Neither of them contributed to the scientific content or interpretation of our results. The final version of this manuscript was thoroughly reviewed and revised by all the authors, who are responsible for all content.

**Acknowledgments**

Our sincere thanks to Alejandra Gonzalez, Lihong Yin, Stephen Shepherd, Stefan Schaffelhofer, Bartolomie Halibart, Farid Aboharb, Sofia Landi & the Freiwald Lab; RU Veterinary Staff, especially Leslie Diaz for surgical support; Jim Hudspeth and Brian Fabella for their inspiration and support; Saskia Haegens, Artyom Astafurov and José Vergara for thoughtful discussions on data analysis

and encouragement. This work was supported by the 1) Charles H. Revson & Leon Levy Foundation Postdoctoral Fellowships (V. Y.); 2) MSTP grant from the NIGMS NIH # T32GM007739 to the Tri-Institutional MD-PhD Program (I.G.R.); 3) Austrian Science Fund (FWF) Erwin Schrödinger Fellowship J458 (R.E); 4) NINDS Award# R01NS110901 by the Department of the Navy, ONR Award # N00014-20-1-2292 (F.W.A); 5) BSF Award# 2019339 (P. Y.); 6) The research reported in this publication was overall supported by the National Institute Of Neurological Disorders And Stroke of the National Institutes of Health under Award Number R01NS110901. The content is solely the responsibility of the authors and does not necessarily represent the official views of the NIH and the ONR.

**Author contributions:**
Conceived and designed the experiments: V.Y., I.G.R., P.Y., F.W.A
Performed behavioral, fMRI & electrophysiology experiments: V.Y., I.G.R.
fMRI Targeting: V.Y., I.G.R.
Electrode implantation: R.A.G., S.M.H., V.Y., F.W.A.
Manual Scoring of Videos: V.Y., I.G.R.
Movement Pattern Automatic Algorithm for Videos: Y.F.
Data Analysis: V.Y., R.E.
Wrote the manuscript: V.Y., Y.P., F.W.A.

**Declaration of interests:** Authors declare no competing interests.

## References

1. M. Brecht, W. A. Freiwald, The many facets of facial interactions in mammals. Curr Opin Neurobiol 22, 259-266 (2012).
2. M. Davare, A. Kraskov, J. C. Rothwell, R. N. Lemon, Interactions between areas of the cortical grasping network. Curr Opin Neurobiol 21, 565-570 (2011).
3. B. E. Kilavik, M. Zaepffel, A. Brovelli, W. A. MacKay, A. Riehle, The ups and downs of beta oscillations in sensorimotor cortex. Exp Neurol 245, 15-26 (2013).
4. M. M. Churchland et al., Neural population dynamics during reaching. Nature 487, 51-56 (2012).
5. R. J. Morecraft, K. S. Stilwell-Morecraft, W. R. Rossing, The motor cortex and facial expression: new insights from neuroscience. Neurologist 10, 235-249 (2004).
6. R. M. Muri, Cortical control of facial expression. J Comp Neurol 524, 1578-1585 (2016).
7. R. J. Morecraft, J. L. Louie, J. L. Herrick, K. S. Stilwell-Morecraft, Cortical innervation of the facial nucleus in the non-human primate: a new interpretation of the effects of stroke and related subtotal brain trauma on the muscles of facial expression. Brain 124, 176-208 (2001).
8. P. Cerrato et al., Emotional facial paresis in a patient with a lateral medullary infarction. Neurology 60, 723-724 (2003).
9. R. T. Ross, R. Mathiesen, Images in clinical medicine. Volitional and emotional supranuclear facial weakness. N Engl J Med 338, 1515 (1998).
10. H. C. Hopf, W. Muller-Forell, N. J. Hopf, Localization of emotional and volitional facial paresis. Neurology 42, 1918-1923 (1992).
11. K. F. Muakkassa, P. L. Strick, Frontal lobe inputs to primate motor cortex: evidence for four somatotopically organized 'premotor' areas. Brain Res 177, 176-182 (1979).
12. R. J. Morecraft, G. W. Van Hoesen, Cingulate input to the primary and supplementary motor cortices in the rhesus monkey: evidence for somatotopy in areas 24c and 23c. J Comp Neurol 322, 471-489 (1992).
13. R. J. Morecraft, C. M. Schroeder, J. Keifer, Organization of face representation in the cingulate cortex of the rhesus monkey. Neuroreport 7, 1343-1348 (1996).
14. H. Tokuno, M. Takada, A. Nambu, M. Inase, Reevaluation of ipsilateral corticocortical inputs to the orofacial region of the primary motor cortex in the macaque monkey. J Comp Neurol 389, 34-48 (1997).
15. S. V. Shepherd, W. A. Freiwald, Functional Networks for Social Communication in the Macaque Monkey. Neuron 99, 413-420 e413 (2018).
16. B. Ruszala, K. A. Mazurek, M. H. Schieber, Somatosensory cortex microstimulation modulates primary motor and ventral premotor cortex neurons with extensive spatial convergence and divergence. bioRxiv 10.1101/2023.08.05.552025 (2023).
17. S. Katzner et al., Local origin of field potentials in visual cortex. Neuron 61, 35-41 (2009).

18. B. Pesaran et al., Investigating large-scale brain dynamics using field potential recordings: analysis and interpretation. Nat Neurosci 21, 903-919 (2018).
19. C. Gallego-Carracedo, M. G. Perich, R. H. Chowdhury, L. E. Miller, J. A. Gallego, Local field potentials reflect cortical population dynamics in a region-specific and frequency-dependent manner. Elife 11 (2022).
20. M. Vinck, M. van Wingerden, T. Womelsdorf, P. Fries, C. M. Pennartz, The pairwise phase consistency: a bias-free measure of rhythmic neuronal synchronization. Neuroimage 51, 112-122 (2010).
21. L. Barnett, A. B. Barrett, A. K. Seth, Granger causality and transfer entropy are equivalent for Gaussian variables. Phys Rev Lett 103, 238701 (2009).
22. A. K. Seth, A. B. Barrett, L. Barnett, Granger causality analysis in neuroscience and neuroimaging. J Neurosci 35, 3293-3297 (2015).
23. M. Iwase et al., Neural substrates of human facial expression of pleasant emotion induced by comic films: a PET Study. Neuroimage 17, 758-768 (2002).
24. B. Wild et al., Humor and smiling: cortical regions selective for cognitive, affective, and volitional components. Neurology 66, 887-893 (2006).
25. M. Kern, S. Bert, O. Glanz, A. Schulze-Bonhage, T. Ball, Human motor cortex relies on sparse and action-specific activation during laughing, smiling and speech production. Commun Biol 2, 118 (2019).
26. A. M. Bastos, J. M. Schoffelen, A Tutorial Review of Functional Connectivity Analysis Methods and Their Interpretational Pitfalls. Front Syst Neurosci 9, 175 (2015).
27. P. J. Uhlhaas et al., Neural synchrony in cortical networks: history, concept and current status. Front Integr Neurosci 3, 17 (2009).
28. S. Haegens, J. Vergara, R. Rossi-Pool, L. Lemus, R. Romo, Beta oscillations reflect supramodal information during perceptual judgment. Proc Natl Acad Sci U S A 114, 13810-13815 (2017).
29. M. A. Hagan, B. Pesaran, Modulation of inhibitory communication coordinates looking and reaching. Nature 604, 708-713 (2022).
30. C. Beste, A. Munchau, C. Frings, Towards a systematization of brain oscillatory activity in actions. Commun Biol 6, 137 (2023).
31. N. Kopell, G. B. Ermentrout, M. A. Whittington, R. D. Traub, Gamma rhythms and beta rhythms have different synchronization properties. Proc Natl Acad Sci U S A 97, 1867-1872 (2000).
32. W. Klimesch, alpha-band oscillations, attention, and controlled access to stored information. Trends Cogn Sci 16, 606-617 (2012).
33. S. Haegens, V. Nacher, R. Luna, R. Romo, O. Jensen, alpha-Oscillations in the monkey sensorimotor network influence discrimination performance by rhythmical inhibition of neuronal spiking. Proc Natl Acad Sci U S A 108, 19377-19382 (2011).
34. M. Siegel, T. H. Donner, A. K. Engel, Spectral fingerprints of large-scale neuronal interactions. Nat Rev Neurosci 13, 121-134 (2012).
35. N. Kopell, M. A. Whittington, M. A. Kramer, Neuronal assembly dynamics in the beta1 frequency range permits short-term memory. Proc Natl Acad Sci U S A 108, 3779-3784 (2011).
36. B. Spitzer, S. Haegens, Beyond the Status Quo: A Role for Beta Oscillations in Endogenous Content (Re)Activation. eNeuro 4 (2017).
37. E. Rassi et al., Distinct beta frequencies reflect categorical decisions. Nat Commun 14, 2923 (2023).
38. C. Constantinidis, A. A. Ahmed, J. D. Wallis, A. P. Batista, Common Mechanisms of Learning in Motor and Cognitive Systems. J Neurosci 43, 7523-7529 (2023).
39. B. Pesaran, M. J. Nelson, R. A. Andersen, Free choice activates a decision circuit between frontal and parietal cortex. Nature 453, 406-409 (2008).
40. O. Dal Monte, C. C. J. Chu, N. A. Fagan, S. W. C. Chang, Specialized medial prefrontal-amygdala coordination in other-regarding decision preference. Nat Neurosci 23, 565-574 (2020).
41. G. Ariani, J. A. Pruszynski, J. Diedrichsen, Motor planning brings human primary somatosensory cortex into action-specific preparatory states. Elife 11 (2022)
42. J. Barone, H. E. Rossiter, Understanding the Role of Sensorimotor Beta Oscillations. Front Syst Neurosci 15, 655886 (2021).
43. N. Dolensek, D. A. Gehrlach, A. S. Klein, N. Gogolla, Facial expressions of emotion states and their neuronal correlates in mice. Science 368, 89-94 (2020).
44. K. M. Gothard, The amygdalo-motor pathways and the control of facial expressions. Front Neurosci 8, 43 (2014).
45. Z. Yang, W. A. Freiwald, Encoding of dynamic facial information in the middle dorsal face area. Proc Natl Acad Sci U S A 120, e2212735120 (2023).
46. F. P. Leite et al., Repeated fMRI using iron oxide contrast agent in awake, behaving macaques at 3 Tesla. Neuroimage 16, 283-294 (2002).
47. Salem KS, Logothetis NK (2007) A combined MRI and Histology Atlas of the Rhesus Monkey Brain in Stereotaxic Coordinates (Academic Press, London UK), 1st Ed.

48. R. Oostenveld, P. Fries, E. Maris, J. M. Schoffelen, FieldTrip: Open source software for advanced analysis of MEG, EEG, and invasive electrophysiological data. Comput Intell Neurosci 2011, 156869 (2011).
49. M. Dhamala, G. Rangarajan, M. Ding, Estimating Granger causality from fourier and wavelet transforms of time series data. Phys Rev Lett 100, 018701 (2008).
50. A. A. Ghazanfar, D. Y. Takahashi, N. Mathur, W. T. Fitch, Cineradiography of monkey lip-smacking reveals putative precursors of speech dynamics. Curr Biol 22, 1176-1182 (2012).
51. M. Petrides, G. Cadoret, S. Mackey, Orofacial somatomotor responses in the macaque monkey homologue of Broca's area. Nature 435, 1235-1238 (2005).

## Figures and Tables

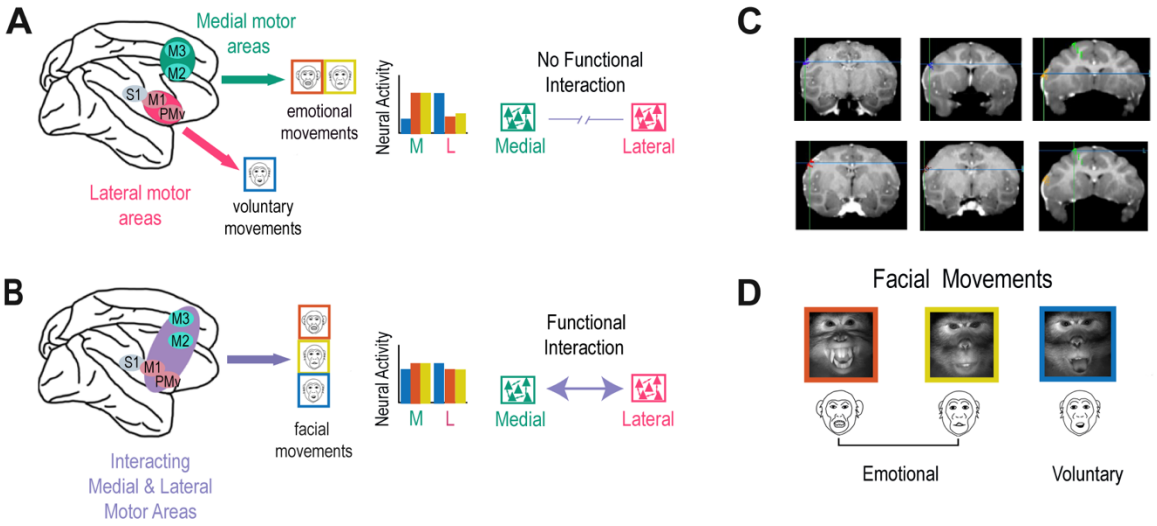


**Figure1. Cortical facial motor representations in the primate brain and facial motor behaviors.** Medial (green) and lateral (pink) motor systems are hypothesized to support emotional and voluntary facial movements, respectively. Two possible neural mechanisms for facial movements are proposed: (**A**) Null hypothesis: medial and lateral motor areas operate independently, with medial regions specialized in emotional movements- facial expressions, and lateral areas for voluntary movements such as chewing. (**B**) Alternative hypothesis: medial and lateral motor areas functionally interact to support both emotional and voluntary movements. (**C**) Structural MRI (T1, coronal plane) showing electrode array placement in one monkey. Floating microarrays targeted primary somatosensory (S1, purple), motor (M1, light & dark red) cortex, ventrolateral premotor (PMv, blue & yellow) and cingulate motor cortex (M3, green). Array locations were based on fMRI conjunction maps of facial expressions and mouth movement (see methods). **(D)** Examples of naturalistic facial movements: threat (red), a non-affiliative emotional display with sustained open mouth; lip-smack (yellow), a rhythmic affiliative emotional movement of jaw and lips; and chewing (blue), an ingestive voluntary movement. Corresponding cartoons below each photo are used as references through the text. Neural activity was recorded simultaneously across all areas during these behaviors, with emotional movements elicited through videos, an avatar and primate interactions (see methods)

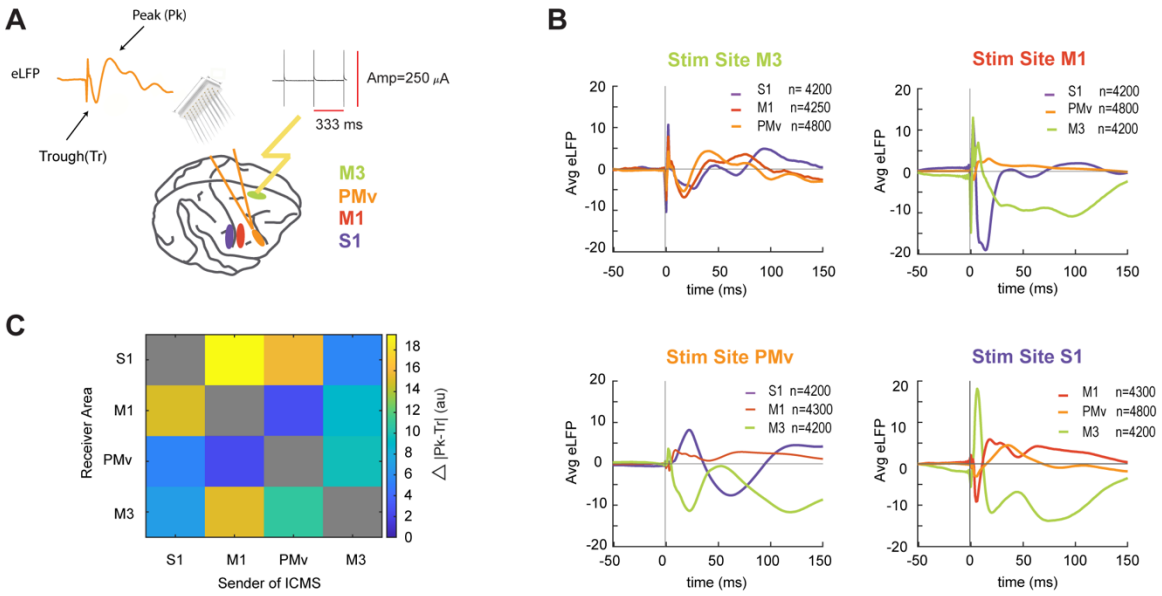


**Figure 2. Mapping Facial Sensory and Motor Connectivity through Intracortical Microstimulation**. (**A**) Illustration depicting a monkey's brain with electrode arrays in the recorded areas. The intracortical microstimulation (ICMS) current protocol was applied to the sender area, in this case the M3 cingulate motor area. The protocol uses a biphasic pulse (250 μA, 0.4 ms duration, at 300 Hz for 2 minutes). The orange trace represents the PMv's mean evoked local field potential due to current propagation, highlighting the first peak and trough after the stimulation onset. (**B**) Averaged evoked local field potentials (LFPs) across cortical areas in response to microstimulation of M3, M1, PMv and S1 cortices. The stimulation onset is marked at zero on the x-axis. A stimulation artifact with rapid onset and large amplitude is visible across all averages during the first few milliseconds following stimulation. This artifact was excluded from the analysis. (**C**) Confusion matrix depicting connectivity indexes measured by the absolute difference between the first peak or trough, and the second trough or peak, respectively (Δ|Peak-Trough|). Current sender areas are shown on the *X*-axis and receiver areas on the *Y*-axis. Gray diagonal elements represent untested within-area connectivity, while off-diagonal elements show the measured connectivity strength.

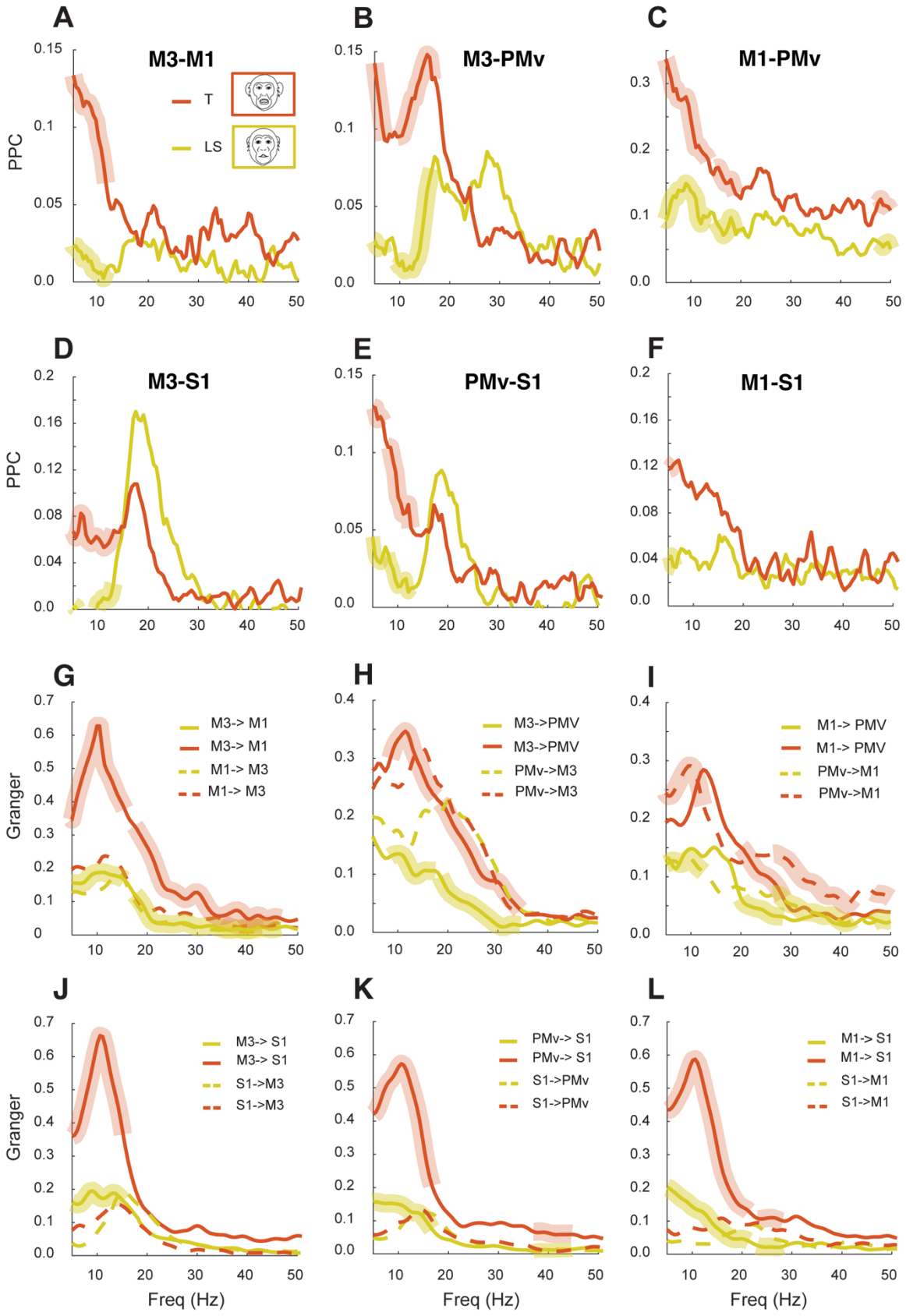
A
M3-M1
T
LS
PPC
B
M3-PMv
C
M1-PMv
D
M3-S1
PPC
E
PMv-S1
F
M1-S1
G
M3-> M1
M3-> M1
M1-> M3
M1-> M3
Granger
H
M3->PMV
M3->PMV
PMv->M3
PMv->M3
I
M1-> PMV
M1-> PMV
PMv->M1
PMv->M1
J
M3-> S1
M3-> S1
S1->M3
S1->M3
Granger
K
PMv-> S1
PMv-> S1
S1->PMv
S1->PMv
L
M1-> S1
M1-> S1
S1->M1
S1->M1
Freq (Hz)
Freq (Hz)
Freq (Hz)

**Figure 3. Functional interactions between facial motor and sensorimotor cortices during the production of emotional facial movements. A-F** Pairwise phase consistency (PPC) between M3 and M1 (medial and lateral motor areas), M3 and PMv (medial and lateral motor areas), M1 and PMv (lateral motor areas), M3 and S1 (medial motor and primary somatosensory area), PMv and S1 (lateral and primary somatosensory area), M1 and S1 (lateral motor and primary somatosensory area) during the production of threats (T: red solid lines, n=1200) and lipsmacks (LS: yellow solid lines, n=1200). In Panels A-F thicker, semi-transparent lines atop the solid lines denote regions of statistical differences between both facial expressions ($p \leq 0.05$). **G-L** Granger causality for pairs of areas: M3-M1, M3-PMv, M1-PMv, M3-S1, PMv-S1, M1-S1 respectively. Solid lines depict a particular directionality of Granger causality (e.g., M3 to M1), while dashed lines depict the opposite direction (e.g. M1 to M3). Thicker semi-transparent lines indicate Granger causality values statistically different between the facial movements.

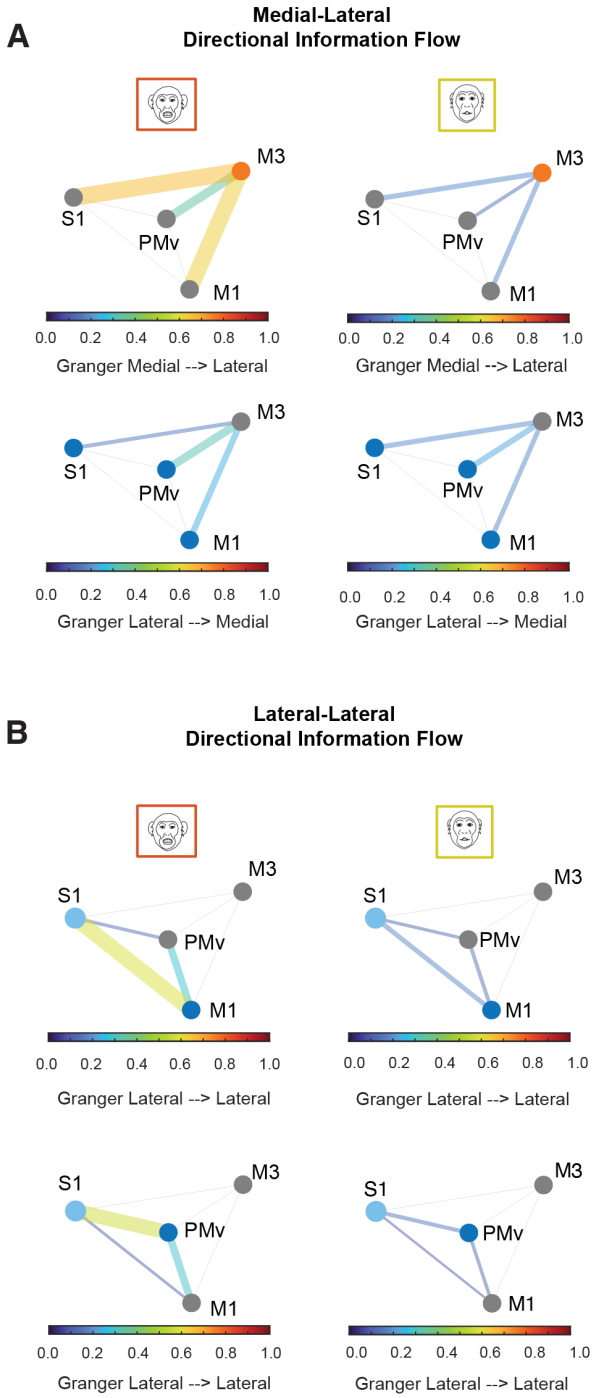


**Figure 4.** Summary of Network analysis during facial expressions. **A-B.** Summary network diagram depicting the Granger's Causality maximum peak between each pair of motor areas and S1 during threats (left panel) and lipsmacks (right panel). Color and thickness of the line indicate the flow's maximum magnitude for each direction. (**A**) Medial-Lateral Directional Information Flow: The upper panel depicts the flow from medial (M3, orange node) to lateral motor and S1 areas, while the lower panel shows flow from lateral areas (M1-PMV-S1, blue nodes) to medial motor area (M3). (**B**) Lateral-Lateral Directional Information Flow: Upper panel depicts flow from M1 to lateral motor areas (PMv and S1), while the lower panel shows flow from area PMv (blue node) to M1 and S1.

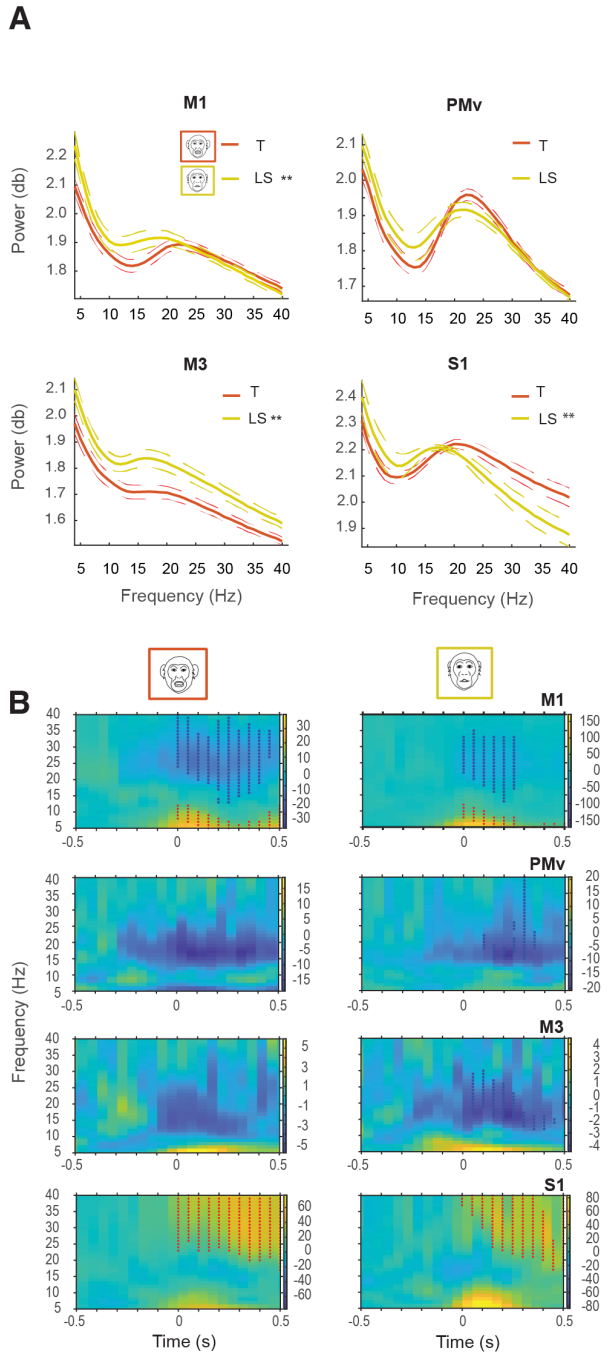


**Figure 5. Local oscillatory activity within motor face and S1 areas for emotional facial movements. (A).** Raw power around the movement onset (±1s) for threats (T: red) and lip-smacks (LS: yellow) in M1, PMv, M3 and S1. Alpha (α = 8-12Hz) and beta (β = 13-40 Hz) activity was modulated across all behaviors. Asterisks indicate significant power differences in α and β ranges between threats and LS (p≤0.01, Kruskal-Wallis test corrected for multiple comparisons, df=2, n=2 monkeys, T=432, LS=292). **(B).** Time frequency representations (TFR, 5-40 Hz) normalized to pre-movement epoch for threats and lipsmacks in M1, PMv, M3, and S1. Time zero indicates movement onset. Asterisks show significant clusters (p≤0.05, cluster-corrected nonparametric randomization test) comparing pre-movement (-0.75 to -0.25s) versus movement epochs (0.0 to 0.5s). Red asterisks denote activity increases, blue asterisks indicate decreases relative to baseline.

**Table 1. Peak Coupling Frequency Among Motor Circuits**

| Movement Type | Gesture | Lateral-Lateral Circuit (M1-PMv) | Medial-Lateral Circuit (M3-M1) | Medial-Lateral Circuit (M3-PMv) |
|---|---|---|---|---|
| | | θ = 7.5, 6.5 Hz, | | |
| **Emotional** | **Lip-Smacking** | α = 9 Hz | | α = 8.5 Hz |
| | | β = 25, 14 Hz | β = 17.5, 23.5 Hz | β = 27.5, 17 Hz |
| | | γ = 46 Hz | γ = 45 Hz | |
| | | | | |
| | | θ = 7 Hz | θ = 7.5 Hz | |
| | **Threat** | α =9 Hz, | α = 13.5 Hz | α = 9,8 Hz |
| | | β= 15.5, 24 Hz | β = 21,33.5 Hz | β = 15, 12 Hz |
| | | γ = 41 Hz | γ= 40 Hz | |
| | | | | |
| | | | | |
| **Voluntary** | **Chew** | θ = 5, 7.5 Hz | θ = 5 Hz, | θ = 5 Hz |
| | | α= 10, 11 Hz | | |
| | | β= 26, 23.5 Hz | β=37, 30 Hz | β=24 Hz |
| | | γ = 44 Hz | γ = 43 Hz | γ = 43.5 Hz |

## Supplementary Information

**A**

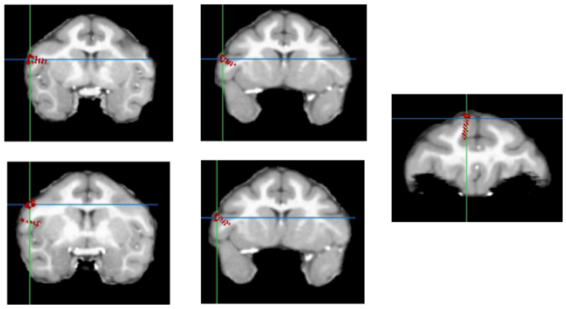

**Fig. S1. Anatomical locations of the arrays in the monkey's brain. (A)** Structural MRI (T1, coronal plane) and overlay showing electrode targeting for each array in the second monkey. Floating microarrays were placed over the primary somatosensory (S1) and motor (M1) cortex, ventrolateral premotor (PMv) and cingulate motor cortex (M3).

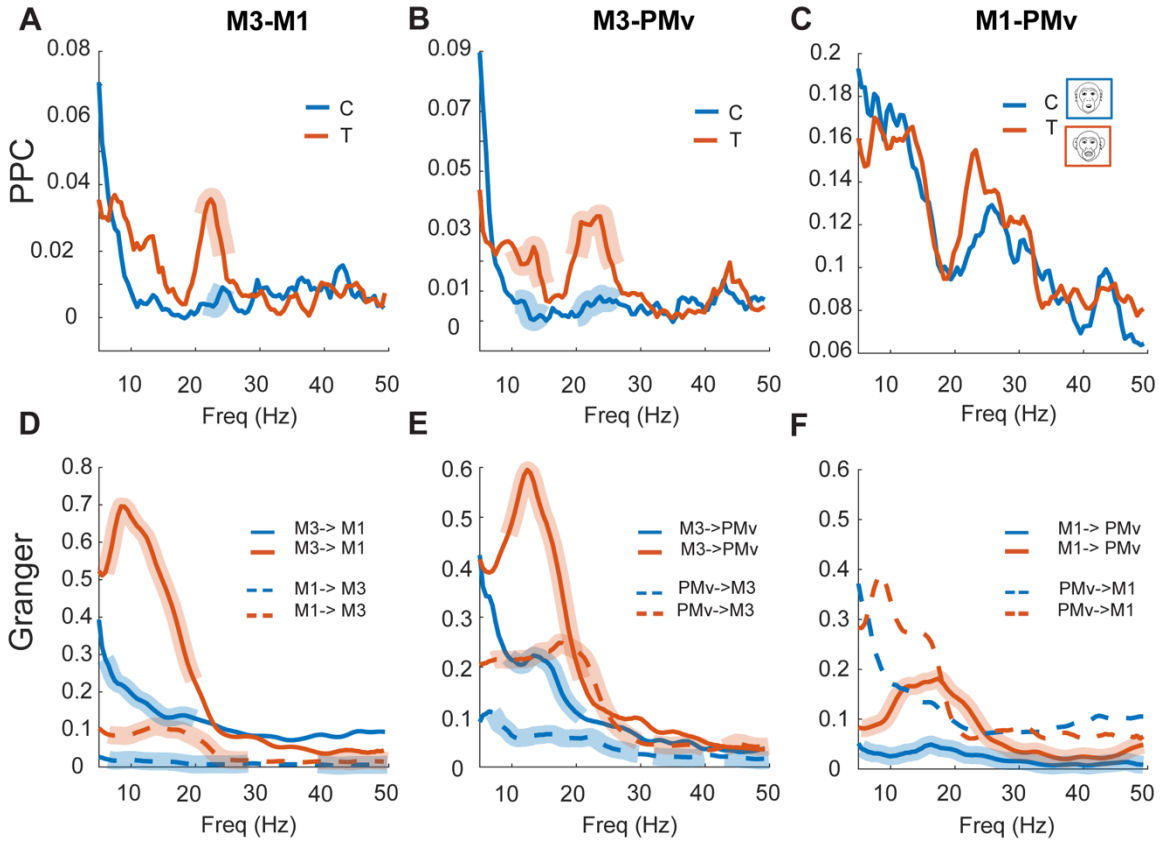


**Fig. S2. Functional interactions between medial and lateral motor areas during voluntary movements. A-C.** Pairwise phase consistency (PPC) between M3-M1, M3-PMv, and M1-PMv, during the production of threats (T: red solid lines) and voluntary chew movements (C: blue solid lines). In Panels A & B thicker, semi-transparent lines atop the solid lines denote regions of statistical differences between both facial movements ($p \leq 0.05$). Non-affiliative facial expressions -threats, depict higher coupling on the beta range between medial and lateral areas than voluntary chew movements. The coupling between lateral areas was not significantly different when comparing both movements. **D-F.** Granger causality for pairs of areas: M3-M1, M3-PMv, and M1-PMv, from left to right. Solid lines depict a particular directional flow e.g. M3 to M1, while dashed lines depict the opposite direction, e.g. M1 to M3. The peak frequency and directional flow pattern within each combination of areas relate to the type of facial movement produced. Thicker semi-transparent lines indicate Granger causality values statistically different between the facial movements.

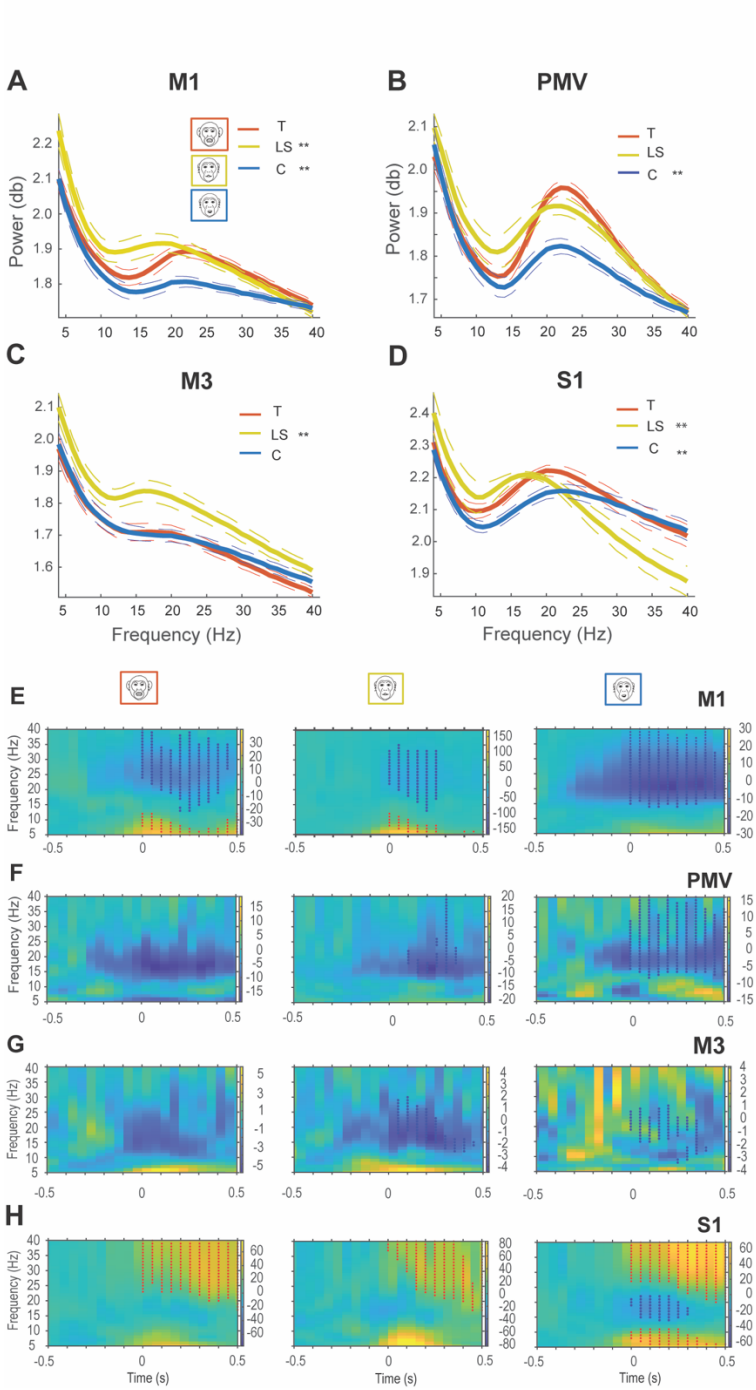


**Fig. S3. Oscillatory activity within the sensory and motor face areas for emotional and voluntary facial movements. A-D** Raw power around the movement onset (±1s) for threats (T: red), lip-smacks (LS: yellow) and chews (C: blue) in M1 (**A**), PMv (**B**), M3 (**C**) and S1(D). Alpha (α = 8-12Hz) and beta (β = 13-40 Hz) activity was modulated across all behaviors. Asterisks indicate significant power differences in α and β ranges between threats and other behaviors (p≤0.01, Kruskal-Wallis test corrected for multiple comparisons, df=2, n=2 monkeys, T=432, LS=292, C=415). **E-H** Time frequency representations (TFR, 5-40 Hz) normalized to pre-movement epoch for threats, lipsmacks and chews in M1 (**E**), PMv (**F**), M3 (**G**), and S1 (**H**). Time zero indicates movement onset. Asterisks show significant clusters (p≤0.05, cluster-corrected nonparametric randomization test) comparing pre-movement (-0.75 to -0.25s) versus movement epochs (0.0 to 0.5s). Red asterisks denote activity increases, blue asterisks indicate decreases relative to baseline.

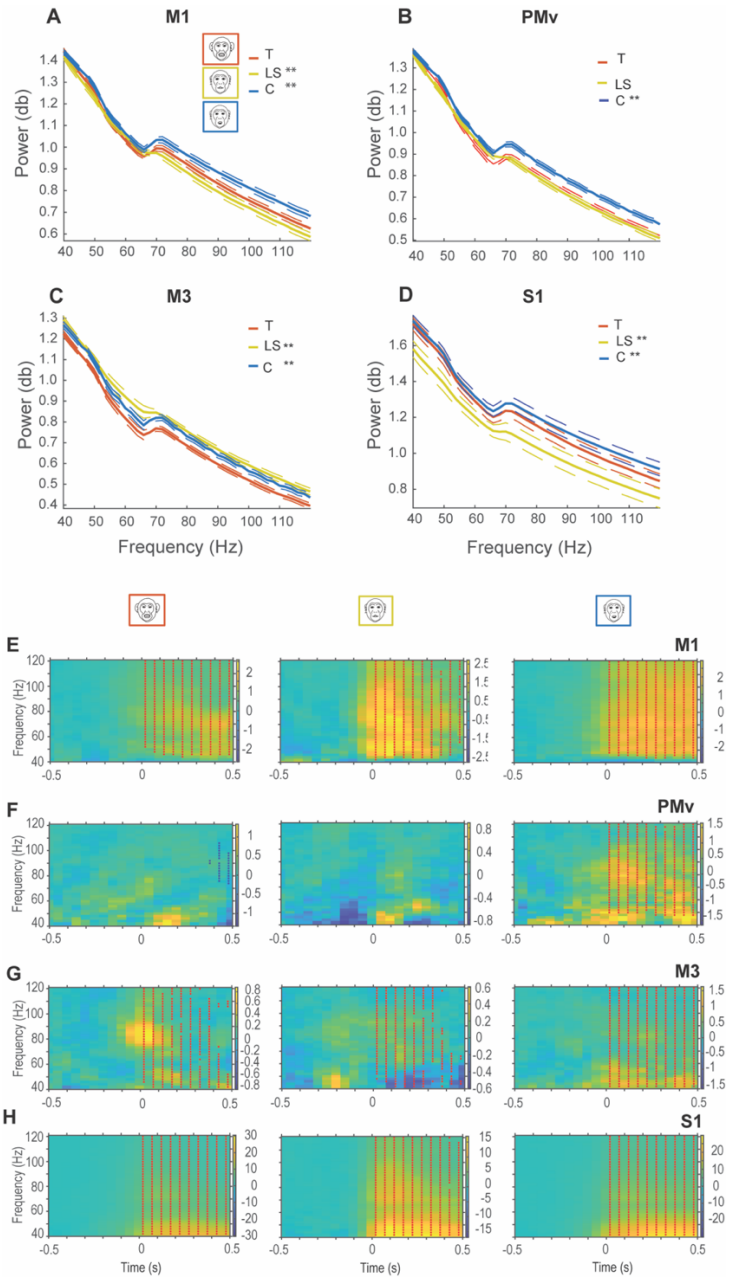


**Fig. S4. Oscillatory activity (40-120Hz) within sensory and motor face areas during emotional and voluntary facial movements. A-D** Raw power around movement onset (±1s) for threats (T: red), lip-smacks (LS: yellow) and chews (C: blue) in: M1 (**A**), PMv (**B**), M3 (**C**) and S1 (**D**). Asterisks indicate significant power differences in gamma range (40-120 Hz) between threats and other behaviors (p≤0.01, Kruskal-Wallis test corrected for multiple comparisons, df=2, n=2 monkeys, T=432, LS=292, C=415). **E-H.** Time frequency representations normalized to pre-movement epoch (-0.75 to -0.25s) for threats, lipsmacks and chews in M1(**E**), PMv(**F**), M3(**G**) and S1(**H**) areas. Asterisks indicate significant clusters (p≤0.05, cluster-corrected nonparametric randomization test, Oostenveld R 2007) comparing pre-movement (-0.75 to -0.25s) versus movement epoch (0.0 to 0.5s). Red asterisks denote power increases, blue asterisks decreases relative to baseline.

**Table S1. PPC during Facial Movement *vs* Rest**

| Facial Movement | Area Pair | Frequency Range | pvalue | Permutations |
|---|---|---|---|---|
| LS | M1-PMV | 18.5 - 20 Hz | p≤ 0.05 | 1000 |
| LS | M1-M3 | 16-18 Hz | p≤ 0.05 | 1000 |
| LS | M3-PMV | 31-33.5 Hz | p≤ 0.05 | 1000 |
| LS | M1-S1 | 40-40.5 Hz | p=0.13 | 1000 |
| LS | M3-S1 | 12-16.5 Hz | p≤ 0.05 | 1000 |
| LS | PMV-S1 | 14.5-17 Hz | p≤ 0.05 | 1000 |
| | | | | |
| T | M1-PMV | 22-24.5 Hz | p≤ 0.05 | 1000 |
| T | M1-M3 | 28.5-29 Hz | p=0.15 | 1000 |
| T | M3-PMV | 19-21.5, 35-36.5 Hz | p=0.07 | 1000 |
| T | M1-S1 | 37.5-39 Hz | p≤ 0.05 | 1000 |
| T | M3-S1 | 12-15 Hz | p≤ 0.05 | 1000 |
| T | PMV-S1 | Tendency in ß range | p>0.05 | 1000 |
| | | | | |
| C | M1-PMV | 4-19Hz | p≤ 0.05 | 1000 |
| C | M1-M3 | 4-11 Hz | p≤ 0.05 | 1000 |
| C | M3-PMV | 4-15.5 Hz | p≤ 0.05 | 1000 |
| C | M1-S1 | 30-32 Hz | p≤ 0.05 | 1000 |
| C | M3-S1 | 4-8 Hz | p≤ 0.05 | 1000 |

*Facial Movement: LS (Lipsmack); T(Threat); C(Chew)

**Table S2. PPC Among Facial Movements**

| Facial Movements | Area Pair | Frequency Range | pvalue | Permutations |
|---|---|---|---|---|
| T vs LS | M1-PMV | 4-13.5 Hz | p≤0.03 | 1000 |
| | | 15-19 Hz | p≤0.017 | 1000 |
| | | 47.5-50 Hz | p≤0.035 | 1000 |
| | | | | |
| T vs LS | M3-M1 | 4-11 Hz | p≤0.003 | 1000 |
| | | | | |
| T vs LS | M3-PMV | 4-7 Hz | p≤0.035 | 1000 |
| | | 9.5-16.5 Hz | p≤0.01 | 1000 |
| | | | | |
| T vs LS | M1-S1 | 4-6.5 Hz | p≤0.0350 | 1000 |
| | | | | |
| T vs LS | M3-S1 | 4-13 Hz | p≤0.0009 | 1000 |
| | | | | |
| T vs LS | PMV-S1 | 4-7 Hz | p≤0.011 | 1000 |
| | | 8-12.5 Hz | p≤0.020 | 1000 |
| | | | | |
| T vs C | M1-PMV | ----- | p>0.05 | 1000 |
| | | | | |
| T vs C | M3-M1 | 21.5-24.5Hz | p≤0.0009 | 1000 |
| | | | | |
| T vs C | M3-PMV | 10.5-15 Hz | p≤0.007 | 1000 |
| | | 20-26 Hz | p≤0.003 | 1000 |

*Facial Movement: LS (Lipsmack); T(Threat); C(Chew)

**Table S3. Granger Causality Among Facial Movements**

| Facial Movements | Direction | Frequency Range | pvalue | Permutations |
|---|---|---|---|---|
| T vs LS | M1 to PMV | 20-28.5 Hz | p≤0.011 | 1000 |
| | | | | |
| T vs LS | PMV to M1 | 4-12.5 Hz | p≤0.018 | 1000 |
| | | 26.5-42.5 Hz | p≤0.007 | 1000 |
| | | 46.5-50 Hz | p≤0.043 | |
| | | | | |
| T vs LS | M1 to M3 | 35-43Hz | p≤0.008 | 1000 |
| | | | | |
| T vs LS | M3 to M1 | 4-15.5 Hz | p≤0.009 | 1000 |
| | | 17.5-46.5 Hz | p≤0.0009 | 1000 |
| | | | | |
| T vs LS | M3 to PMV | 8.5-17.5 Hz | p≤0.02 | 1000 |
| | | 18.5-34.5 Hz | p≤0.007 | 1000 |
| | | | | |
| T vs LS | PMV to M3 | ------ | p>0.05 | 1000 |
| | | | | |
| T vs LS | M1 to S1 | 4-21 Hz | p≤0.002 | 1000 |
| | | 23-28 Hz | p≤0.0230 | 1000 |
| | S1 to M1 | ------ | | |
| | | | | |
| T vs LS | M3 to S1 | 4-15 Hz | p≤0.0060 | 1000 |
| | S1 to M3 | ------- | | |
| | | | | |
| T vs LS | PMV to S1 | 4-16.5 Hz | p≤0.0100 | 1000 |
| | | 37-44.5 Hz | p≤0.0230 | 1000 |

| | | | | |
|---|---|---|---|---|
| | S1 to PMV | ----- | | |
| | | | | |
| T vs C | M1 to PMV | 5.5-50 Hz | $p \leq 9.99X10^{-4}$ | 1000 |
| | | | | |
| | PMV to M1 | ---- | $p > 0.05$ | 1000 |
| | | | | |
| T vs C | M1 to M3 | 6.5-28.5 Hz | $p \leq 9.99X10^{-4}$ | 1000 |
| | | 39-50 Hz | $p \leq 0.008$ | 1000 |
| | | | | |
| | M3 to M1 | 6-20 Hz | $p \leq 0.017$ | 1000 |
| | | | | |
| T vs C | M3 to PMV | 9.5-21 Hz | $p \leq 0.02$ | 1000 |
| | | | | |
| | PMV to M3 | 7-30 Hz | p≤9.99X10-4 | 1000 |
| | | 32-40 Hz | $p \leq 0.31$ | 1000 |
| | | 43-50 Hz | $p \leq 0.023$ | 1000 |

*Facial Movement: LS (Lipsmack); T(Threat); C(Chew)

**Table S4. Power across Different Facial Movements (8-40Hz)**

| Brain Area, Movements | Diff [95% CI] | pvalue |
|---|---|---|
| S1, T-LS | 214.91 [117.63, 312.19] | ≤0.001 |
| S1, T-C | 177.03 [102.72, 251.35] | ≤0.001 |
| S1, LS-C | -37.88 [-134.62, 58.87] | 0.629 |
| | | |
| M1, T-LS | -182.86 [-280.14, -85.58] | ≤0.001 |
| M1, T-C | 312.85 [238.53, 387.16] | ≤0.001 |
| M1, LS-C | 495.71 [398.97, 592.45] | ≤0.001 |
| | | |
| PMv, T-LS | -64.61 [-161.89, 32.67] | 0.265 |
| PMv, T-C | 366.00 [291.68, 440.31] | ≤0.001 |
| PMv, LS-C | 430.61 [333.87, 527.35] | ≤0.001 |
| | | |
| M3, T-LS | -578.57 [-675.85, -481.29] | ≤0.001 |
| M3,T-C | -54.03 [-128.34, 20.29] | 0.204 |
| M3, LS-C | 524.54 [427.80, 621.29] | ≤0.001 |

*Facial Movement: LS (Lipsmack); T(Threat); C(Chew)

**Table S5. Power across Different Facial Movements (40-120Hz)**

| Brain Area, Movements | Diff [95% CI] | pvalue |
|---|---|---|
| S1, T-LS | 388.86 [295.39, 482.33] | ≤0.001 |
| S1, T-C | -116.27 [-187.67, -44.87] | ≤0.001 |
| S1, LS-C | -505.13 [-598.08, -412.18] | ≤0.001 |
| | | |
| M1, T-LS | 179.80 [86.33, 273.26] | ≤0.001 |
| M1, T-C | -308.16 [-379.56, -236.75] | ≤0.001 |
| M1, LS-C | -487.95 [-580.90, -395.00] | ≤0.001 |
| | | |
| PMv, T-LS | 69.72 [-23.74, 163.19] | 0.187 |
| PMv, T-C | -431.00 [-502.41, -359.60] | ≤0.001 |
| PMv, LS-C | -500.73 [-593.68, -407.78] | ≤0.001 |
| | | |
| M3, T-LS | -601.64 [-695.10, -508.17] | ≤0.001 |
| M3,T-C | -388.80 [-460.20, -317.39] | ≤0.001 |
| M3, LS-C | 212.84 [119.89, 305.79] | ≤0.001 |

*Facial Movement: LS (Lipsmack); T(Threat); C(Chew)